HHS Public Access

Author manuscript

RSC Adv. Author manuscript; available in PMC 2016 December 01.

Published in final edited form as:

RSC Adv. 2015 ; 5(128): 105551–105559. doi:10.1039/C5RA16305F.

Targeting bacterial biofilms via surface engineering of gold nanoparticles

Karuna Giri[1], **Laura Rivas Yepes**[2,3], **Bradley Duncan**[4], **Praveen Kolumam Parameswaran**[2], **Bo Yan**[4], **Ying Jiang**[4], **Marcela Bilska**[2,3], **Daniel F. Moyano**[4], **Mike Thompson**[2,3], **Vincent M. Rotello**[4], and **YS Prakash**[2,3]

[1]Department of Biochemistry and Molecular Biology, Mayo Clinic, 200 1st St SW, Rochester, MN 55905

[2]Department of Anesthesiology, Mayo Clinic, 200 1st St SW, Rochester, MN 55905

[3]Department of Physiology & Biomedical Engineering, Mayo Clinic, 200 1st St SW, Rochester, MN 55905

[4]Department of Chemistry, University of Massachusetts Amherst, 710 North Pleasant Street, Amherst, Massachusetts 01003, United States

Abstract

Bacterial biofilms are associated with persistent infections that are resistant to conventional antibiotics and substantially complicate patient care. Surface engineered nanoparticles represent a novel, unconventional approach for disruption of biofilms and targeting of bacterial pathogens. Herein, we describe the role of surface charge of gold nanoparticles (AuNPs) on biofilm disruption and bactericidal activity towards *Staphylococcus aureus* and *Pseudomonas aeruginosa* which are important ventilator associated pneumonia (VAP) pathogens. In addition, we study the toxicity of charged AuNPs on human bronchial epithelial cells. While 100% positively charged AuNP surface was uniformly toxic to both bacteria and epithelial cells, reducing the extent of positive charge on the AuNP surface at moderate concentrations prevented epithelial cell toxicity. Reducing surface charge was however also less effective in killing bacteria. Conversely, increasing AuNP concentration while maintaining a low level of positivity continued to be bactericidal and disrupt the bacterial biofilm and was less cytotoxic to epithelial cells. These initial *in vitro* studies suggest that modulation of AuNP surface charge could be used to balance effects on bacteria vs. airway cells in the context of VAP, but the therapeutic window in terms of concentration vs. surface positive charge may be limited. Additional factors such as hydrophobicity may need to be considered in order to design AuNPs with specific, beneficial effects on bacterial pathogens and their biofilms.

INTRODUCTION

Ventilator-associated pneumonia (VAP) is one of the most common hospital acquired infections, and is associated with increased duration of mechanical ventilation, prolonged intensive care unit (ICU) and hospital stay as well as increased mortality in the ICU.[1–8] Common pathogens implicated in VAP include species from the *Staphylococcaceae*, *Streptococcaceae*, *Pseudomonadaceae*, *Enterobacteriaceae*, and *Pasteurellaceae*

families.[9–12] In this regard, the endotracheal tube (ETT) is a major risk factor for VAP as it provides pathogens with a conducive environment to produce robust biofilms: well-recognized microbial assemblies associated with persistent infection and often highly resistant to conventional antibiotics.[13, 14] Accordingly, targeting of pathogens within the biofilm is critical to resolution of VAP, but presents a significant challenge because the bacteria are encased in a matrix of extracellular polymeric substances (EPS) that inhibit the penetration of antibiotic agents and further promote antibiotic resistance.[15–17] While current ETT design modifications such as silver impregnation and surface rendering have been helpful in slowing biofilm formation, alternative approaches are needed for biofilm penetration with bactericidal effects.[6, 18, 19]

Nanoparticles provide a unique strategy to target bacterial biofilms, with the potential to use both antibiotic-free and antibiotic-coated approaches.[20–22] With regard to the former, the biological activity of nanoparticles *per se* is dependent on a number of factors, including the core material, size and in particular engineered surface properties such as charge and hydrophobicity.[23–25] The unique properties of nanoparticles have been utilized for identification and targeting of various bacterial biofilms. [26–28] However, an important consideration is the balance between bactericidal (or bacteriostatic) activity vs. host cytotoxicity, i.e. adverse effects on lung epithelial and other cells in the case of VAP. There are currently limited data exploring the relationships between nanoparticle surface properties and their ability to be concurrently bactericidal and non-cytotoxic.[29, 30] In this study, we investigated the use of surface engineered gold nanoparticles (AuNPs) for targeting of VAP-associated pathogens. We previously showed that surface charge can be modulated to penetrate bacterial biofilms.[29] However, it was observed that while cationic nanoparticles are toxic towards bacteria, they are also toxic towards human cells.[31, 32] Accordingly, in this study, we proposed that modulation of surface positive charge allows for achieving specific toxicity towards bacterial biofilms while minimizing mammalian cytotoxicity. We tested the toxicity of nanoparticles possessing different surface charges against an experimental biofilm model of *Staphylococcus aureus* and *Pseudomonas aeruginosa*: pathogens known to cause VAP.[12] We also compared the cytotoxicity of such AuNPs towards human bronchial epithelial cells in the context of potential future application in targeting VAP-associated pathogens on ETTs in intubated patients.

MATERIALS AND METHODS

Synthesis and characterization of AuNPs

The ligands (TTMA, TEGOH) and the core AuNPs were synthesized according to previously reported methods.[33, 34] Briefly, pentanethiol-coated AuNPs with core diameters of ~2 nm were synthesized using the Brust–Schiffrin two-phase synthesis method. Subsequently, the Murray place-exchange method was used to functionalize AuNPs of desired surface charge ratio. In a typical reaction to create differentially charged nanoparticles, 10 mg of pentanethiol-Au was dissolved in 10 mL of distilled dichloromethane (DCM) and purged with argon for 10 min. Subsequently, 50 mg of TTMA and TEGOH ligand was added to the nanoparticle solution. Different percentages of positive charge were attained by varying TTMA: TEGOH ligand ratio. The reaction mixture was

stirred for 2 d followed by removal of the solvent mixture. The resulting black colored residue was then washed with DCM 5 times and dialyzed for 72 h against Milli-Q water to remove excess ligands. The relative amounts of each ligand on each nanoparticle were determined by laser desorption/ionization mass spectrometry (LDI-MS) as previously described.[35] AuNPs were further characterized using transmission electron microscopy (TEM) and dynamic light scattering (DLS).

Mammalian cell culture

BEAS-2B (human airway epithelial cells) were grown in DMEM/F12 medium (Gibco, 11039-021) supplemented with 1% antibiotics and 10% fetal bovine serum (FBS) and maintained under standard culture conditions (37°C, 5% CO_2). Cells were grown to 80% confluence prior to plating for experiments.

Effect of AuNPs on mammalian cell proliferation

10,000 BEAS-2B cells were plated per well in a 96-well plate and allowed to grow for 24 h after which cells were treated with 100 μl of increasing concentrations of AuNPs (10nM, 100nM or 1 μM). Control cells were treated with media without AuNPs, and wells with 100 μl of media were used as blanks. The effect of AuNP on proliferation of mammalian cells was measured using CyQUANT direct cell proliferation assay (Life Technologies, C35011) according to manufacturer's protocol. Briefly, after 24 or 48 h of exposure to AuNPs, cells were treated with 100 μl of 2x of detection reagent. Cells were incubated for 1 h at 37°C and the fluorescence signal was read on a FlexStation3 microplate reader at 485nm Ex/538 nm Em.

Effect of AuNPs on mammalian cell viability and cell membrane viability

50,000 BEAS-2B cells were plated per well in an 8-well chambered plate (Lab-Tek, 155411) for 24 h after which the cells were treated with 150 μl of increasing concentrations of AuNP (10nM, 100nM or1 μM). Control cells were treated with media free of AuNPs, while cells treated with 70% methanol for 30 min served as a positive control for dead cells. After incubation for 24 h, cells were stained with LIVE/DEAD® viability/cytotoxicity kit (Invitrogen, L3224) per manufacturer's protocol. Briefly, cells were stained with 2 μM calcein AM and 4 μM Ethidium Homodimer-1 (EthD-1) for 30 min. In order to assess AuNP effect on cell membranes (without frank toxicity), 3 h of AuNP exposure was used, allowing for imaging of cells without a wash step (which may loosen and remove affected cells). Images were captured using a Nikon Eclipse Ti microscope and appropriate fluorescence filters. Live cells displayed green fluorescence whereas the nucleus of membrane-compromised cells and that of dead cells displayed red fluorescence.

Bacterial cultures and biofilm formation

Staphylococcus aureus (ATCC, 29213) culture was grown in Tryptic Soy Broth (TSB) without dextrose (BD, 286220). This bacterial strain was selected based on its biofilm-forming ability and its isolation from human wounds (per ATCC specifications). The strain of *Pseudomonas aeruginosa* (ATCC, 27318) used in the study was isolated from human lung and grown in LB broth media. A single bacterial colony was used to inoculate 5 ml of

fresh medium. Bacterial culture was grown at 37°C under constant shaking at 225 rpm. Following incubation, the inoculum density of cells was tested using McFarland turbidity standards. The culture was diluted to 1.0 McFarland and further diluted 1:50 in appropriate growth media before plating for experiments. For a robust biofilm formation of *S. aureus* in 8 and 96-well plates, bacteria were grown in TSB supplemented with 1% glucose. In case of *P. aeruginosa*, bacteria culture was plated in an 8-well chambered plate in LB media. After overnight incubation, the plate was washed with water to remove planktonic bacteria. Fresh LB media was added and the attached biofilm was allowed to grow for another 24 h before experimentation.

Assessment of bacteria viability and cell membrane integrity

100μl of diluted bacterial culture was grown in an 8-well chambered plate for 24 h and treated with increasing concentration of AuNPs (10 nM, 100 nM or 1 μM). AuNP-free medium was added to the control well, while 70% isopropyl alcohol treatment for 30 min was used as a positive control for dead cells. After incubation for 24 h, cells were stained using the LIVE/DEAD® BacLight bacterial viability kit (Life Technologies, L7012) according to manufacturer's protocol. For 3 h AuNP exposure, which specifically examined effects of AuNPs on cell membrane integrity, SYTO9 and PI were prepared along with AuNPs so that a wash step would not be needed, thus decreasing the chance of dislodging and removing affected cells. The excitation/emission maxima used for SYTO9 and PI were 480/500 nm and 490/635 nm, respectively. Bacterial biofilms were imaged using a Nikon Eclipse Ti microscope. SYTO9 is cell permeable and stains all cells green whereas cell-impermeable PI only competitively binds to cells that have lost their membrane integrity. Consequently, live bacteria fluoresce green whereas cells that are dead or have disrupted cell membranes fluoresce red.

Assessment of biofilm formation

50 μl of diluted bacterial culture was plated in a 96-well plate along with AuNPs to achieve final AuNP concentration of 10 nM, 100 nM or 1 μM. Bacteria biofilm grown in media without AuNPs served as a no-treatment control, while wells with media only were used as blanks for the experiment. Plates were incubated for 48 h at 37°C after which the bacterial biofilm was washed to remove planktonic bacteria. The biofilm was then stained with 50 μl of 0.5% crystal violet (Sigma, V5265) at room temperature for 1 h and then thoroughly washed to remove excess dye. After air drying the biofilm, 70 μl of 70% ethanol was used to dissolve the dye. The absorbance from each well was read on the FlexStation3 microplate reader at 595 nm.

Detection of lactate dehydrogenase A (LDHA)

LDHA is an intracellular enzyme that is released upon cell membrane damage. Bacteria and mammalian cells were treated with 1 μM AuNP as described above. After 6 h, the conditioned media from all AuNP-treated wells were collected for enzymatic detection of LDHA. For bacterial cells, the conditioned media were spun at 5000 rpm for 10 min to remove floating cells. Cells treated with media without AuNP were used as control and growth media without any cells were used as blanks for the assay. The amount of LDH

present in the media of control or AuNP treated cells was measured using the LDH Cytotoxicity Colorimetric Assay Kit II (Biovision, K313-500). 30 μl of conditioned media were mixed with 100 μl of reaction mixture and after 30 min of incubation, absorbance was measured at 450nm using FlexStation 3 microplate reader. Absorbance representing the amount of LDH in each of the samples was compared to that of control to quantify fold-changes in LDH release.

RESULTS

To generate nanoparticles that can effectively and selectively target bacterial biofilm, we synthesized AuNPs with differential surface positive charges (Figure 1). The percent of positively charged ligands (TTMA) on AuNP surfaces against neutral ligands (TEGOH) was varied from 100 % to 96 %, 65 %, 20 %, and 0 %.

Characterization of AuNPs

The composition of the percent of TTMA and TEGOH ligands on the AuNP surface was characterized using LDI-MS (Figure 2, Table 1). The zeta potential of 100% TEGOH AuNPs was 1.2 mV while that of other positively charged mixed ligand AuNPs ranged from 24.6 to 27.6 mV (Table 2). The core size of all AuNPs was approximately ~2.5 nm (Table S1). Along with the ligands, the size of AuNPs ranged from 10.2 to 11.5 nm (Table 2).

Effect of AuNPs on the viability of S. aureus

To determine the effect of different percent of AuNP surface positive charge, we first investigated the bactericidal effect of the synthesized AuNPs on *S. aureus* biofilm. The strain of this bacterium was chosen because of its relevance to human disease. We exposed bacterial biofilm to increasing concentrations of AuNPs for 24 h. The neutral AuNPs possessed 100% TEGOH ligands and hence had 0% positivity. The 100% positive charged AuNP contained all TTMA ligands and no TEGOH ligands. Intermediately-charged AuNPs were composed of varying percent of TTMA ligands such as 20%, 65% and 96% with the remaining ligands being TEGOH. The effect of AuNPs on bacterial biofilm was studied by staining bacterial biofilm with SYTO9 and PI (Figure 3). At AuNP concentration of 10 nM and 100 nM, none of the AuNPs exhibited significant bactericidal effect, as evidenced by the presence of uniformly green-fluorescing biofilms. At 1 μM, however, all positively-charged AuNPs decreased bacterial viability. AuNP with 65% TTMA in particular showed substantial bactericidal activity which suggested that a partial positive charge of sufficient concentration was effective in decreasing bacterial viability. Interestingly, neutral AuNPs with 100% TEGOH ligands also resulted in decreased bacterial biofilm, although their bactericidal activity was less than that seen with positively charged AuNPs. Additionally, when biofilms were imaged 3 h after 1 μM AuNP exposure, disruption of the biofilm network was apparent with positively charged AuNPs (Figure S3).

AuNPs disrupt S. aureus biofilm production

To investigate the effect of AuNPs on the production of bacterial biofilm, we quantified the *S. aureus* biofilm using crystal violet staining. Bacterial biofilm was allowed to form for 48 h in the presence of 10 nM, 100 nM or 1 μM AuNP (Figure 4). No significant effects were

observed at 10 nM, whereas at 100 nM only AuNPs with higher percent of positive charge (100% TTMA and 65% TTMA) significantly decreased biofilm production. Comparable with what we previously observed with SYTO9 and PI staining, all AuNPs at 1 μM concentration showed robust decrease in *S. aureus* biofilm. 100% TTMA AuNPs were the most effective at decreasing bacterial biofilm. Other AuNPs including the neutral 100% TEGOH also showed substantial reduction in S. *aureus* biofilm although to a lesser degree.

Cytotoxicity of AuNPs towards human bronchial epithelial cells

We next investigated the cytotoxic effects of AuNPs on human bronchial epithelial cells. We used cell-permeant calcein AM and EthD-1 to visualize live and membrane-compromised cells, respectively. Non-fluorescent calcein AM is enzymatically converted to fluorescent green calcein inside live cells. EthD-1 on the other hand is non-permeable unless the cell membrane is disrupted, and upon binding to DNA results in 40-fold increase in red fluorescence. As shown in the representative images in Figure 5, no apparent toxicity was observed after treatment with 10 nM or 100 nM AuNPs for 24 h. However, at 1 μM concentration, the cytotoxic effect of AuNPs was dependent on the percent of surface positive charge. 100% TEGOH particles (i.e. no positivity) showed no apparent cytotoxic effect to epithelial cells, while 20% TTMA AuNPs only slightly affected the morphology of cells. However, AuNPs with higher percentages of positive charge showed significant cytotoxicity as evidenced by a decrease in cell number and pronounced condensed cell morphology.

Effects of AuNPs on human bronchial epithelial cell proliferation

To investigate further any detrimental effects of AuNPs on human airway cells, in the context of potential use of AuNPs for VAP prevention, we studied the effect of AuNPs on epithelial cell proliferation. We treated cells with increasing concentrations of AuNPs for 24 h and 48 h (Figure 6A and 6B, respectively). After exposure to 10 nM or 100 nM AuNP, cell proliferation was not significantly altered at either time point. However, at 1 μM, all positively charged AuNPs significantly decreased cell proliferation. Even the neutral AuNPs showed significant cytotoxic effect at 48 h.

AuNP treatment damages cell membranes of S. aureus and P. aeruginosa

Based on the finding that 24 h AuNP exposure caused cytotoxicity such that damage to the cell membrane could not be assessed, we used shorter AuNP exposure to study membrane integrity. We stained bacterial biofilm with SYTO9 and PI after 3 h of AuNP treatment. PI only enters membrane compromised cells and hence the presence of red fluorescence stain can be used to visualize cells with disrupted membrane integrity. We also included study of *P. aeruginosa* biofilm to investigate whether bactericidal effects of AuNPs was dependent on peptidoglycan layer present in gram positive bacteria such as *S. aureus*. In addition, *P. aeruginosa* (like *S. aureus*) is an important pathogen implicated in VAP.[6] Compared to control, AuNP-treated bacterial biofilm of both pathogens showed increased red, PI fluorescence suggesting AuNP-related damage to the cell membrane (Figure 7A). We also investigated cell membrane integrity of mammalian cells using calcein AM and EthD-1. Comparable to PI, EthD-1 enters cells that have damaged cell membranes. In contrast to the

results with bacteria, we observed an overall decrease of green fluorescence in 100% TTMA treated cells but no increase in red fluorescence. The absence of cell membrane compromise by AuNPs suggests a unique mechanism of cytotoxicity with positive charged AuNPs. To corroborate these results, we also measured the presence of LDHA in the conditioned media 6 h after treatment with AuNPs (Figure 7B). Taken together, fluorescence analysis and LDHA release by *S. aureus* point to cell membrane damage as a mechanism of AuNP toxicity in bacteria. On the other hand, for mammalian cells, comparably modest increases in LDH after treatment of high-positivity AuNPs, and the lack of EthD-1 staining, suggest cytotoxicity but through a non-cell membrane related mechanism.

DISCUSSION

Surface charge on nanoparticles confers an important characteristic that influences their interaction with cells, and hence also their toxicity against bacteria and mammalian cells. Cationic AuNPs have been previously reported to interact with and aggregate on both Gram-positive and Gram-negative bacterial cell membranes, inhibit bacterial protein synthesis and disrupt cell membranes.[3637] Our results showed that surface positive charge, even at only 20%, may be sufficient to induce toxic effects on bacteria, and significantly decrease formation of bacterial biofilm. Adherent bacteria produce abundant EPS that enclose and protect bacteria from the host's defense mechanisms as well as antibiotics.[16] Previous studies with AuNPs have shown that treatment with AuNPs does not induce bacterial resistance even after treatment over multiple generations.[38] Therefore, prevention of biofilm with positive charged AuNPs provides an attractive strategy for prevention and alleviation of infections, e.g. in the context of VAP. In this regard, an important finding in our study is that surface charge is one factor that would eventually drive the balance between bactericidal activity/biofilm disruption and mammalian cytotoxicity in the context of the lung.

Highly positive AuNPs demonstrated cytotoxic effects towards bronchial epithelial cells and bacterial biofilm in a concentration-dependent manner. Notably, even neutral AuNPs at 1 μM concentration were able to decrease bacterial biofilms. We speculate that the presence of AuNPs disrupts the network of EPS, thus inhibiting expansion of the biofilm. This is consistent with previous reports using surface functionalized silver nanoparticles of positive and neutral charge.[39] The extent of cytotoxicity towards mammalian cells was dependent on the ratio of positively charged ligands, which is consistent with previous findings that positively charged AuNPs depolarize membrane potential and disrupt cell membrane lipid bilayers.[32] We found evidence for cytotoxicity, but interestingly there was no disruption of cell membrane integrity by positively charged AuNPs. Our studies show that even small (20 % TTMA) to moderate (60 %TTMA) positive surface charge at concentrations of 100 nM and 1 μM is sufficient to induce bactericidal effects and disrupt biofilm, however these concentrations demonstrate cytotoxic effects as well. We speculate that additional surface functionality such as hydrophobicity should be considered when designing nanoparticle surfaces that are specifically toxic towards bacterial cells, but are well tolerated by the epithelial lining. Furthermore, additional studies are required to fully understand the relationships between AuNP surface charge and cytotoxicity. Other important considerations for the use of AuNPs in the airway are their effects on epithelial barrier function, the

mechanisms underlying transport of AuNP across the epithelial barrier, and any potential effects of AuNPs on other cell types in the airway, including airway smooth muscle which would influence bronchoconstriction, fibroblasts which influence airway remodeling and fibrosis, and nerves which modulate airway irritability. These issues are topics for future studies before AuNPs can be intelligently and appropriately engineered for targeting bacterial pathogens in VAP.

CONCLUSION

Our findings suggest that positive charge even in small proportions on the nanoparticle surface exhibits antibacterial effects and compromises bacterial cell membranes. However, AuNP concentrations that induce bactericidal effect and disruption of bacterial biofilms also show cytotoxic effects towards human bronchial epithelial cells. In this regard, the therapeutic window in terms of nanoparticle concentration may be narrow and the use for positively charged AuNPs at high concentrations may be limited to a coating layer for use in the ETT lumen. However, modulating surface charge towards lesser positivity in addition to other surface properties such as hydrophobicity could potentially reduce mammalian cytotoxicity, and may thus be used to help design nanoparticles with appropriate safety profiles.

Supplementary Material

Refer to Web version on PubMed Central for supplementary material.

Acknowledgments

Supported by a High-Impact Pilot and Feasibility Award (HIPFA) made possible by Mayo Clinic CTSA Grant Number UL1 TR000135 from the National Center for Advancing Translational Sciences (NCATS), a component of the National Institutes of Health (NH) (Prakash, Rotello) and NIH GM077173 (Rotello).

References

1. Parker CM, Kutsogiannis J, Muscedere J, Cook D, Dodek P, Day AG, Heyland DK. Journal of Critical Care. 2008; 23:18–26. [PubMed: 18359417]
2. Koenig SM, Truwit JD. Clinical Microbiology Reviews. 2006; 19:637–657. [PubMed: 17041138]
3. Stone PW. Expert review of pharmacoeconomics & outcomes research. 2009; 9:417–422. [PubMed: 19817525]
4. Melsen WG, Rovers MM, Groenwold RHH, Bergmans DCJJ, Camus C, Bauer TT, Hanisch EW, Klarin B, Koeman M, Krueger WA, Lacherade JC, Lorente L, Memish ZA, Morrow LE, Nardi G, van Nieuwenhoven CA, O'Keefe GE, Nakos G, Scannapieco FA, Seguin P, Staudinger T, Topeli A, Ferrer M, Bonten MJM. The Lancet Infectious Diseases. 2013; 13:665–671. [PubMed: 23622939]
5. Møller AH, Hansen L, Jensen MS, Ehlers LH. Journal of Medical Economics. 2012; 15:285–292. [PubMed: 22149533]
6. Barbier F, Andremont A, Wolff M, Bouadma L. Current Opinion in Pulmonary Medicine. 2013; 19:216–228. [PubMed: 23524477]
7. Kollef MHH, CW, Ernst FR. Infection Control and Hospital Epidemiology. 2012; 33:250–256. [PubMed: 22314062]
8. Kollef MH. Critical Care Medicine. 2014; 42:2178–2187. [PubMed: 25054674]
9. Kalanuria AA, Zai W, Mirski M. Critical Care. 2014; 18:208–208. [PubMed: 25029020]
10. Park DR. Respiratory Care. 2005; 50:742–765. [PubMed: 15913466]

11. Namiduru M, Güngör G, Karaoğlan I, Dikensoy Ö. Journal of International Medical Research. 2004; 32:78–83. [PubMed: 14997711]
12. Chi SY, Kim TO, Park CW, Yu JY, Lee B, Lee HS, Kim YI, Lim SC, Kwon YS. Tuberculosis and Respiratory Diseases. 2012; 73:32–37. [PubMed: 23101022]
13. Inglis TJ, Millar MR, Jones JG, Robinson DA. Journal of Clinical Microbiology. 1989; 27:2014–2018. [PubMed: 2778064]
14. De Souza PR, De Andrade D, Cabral DB, Watanabe E. Microscopy Research and Technique. 2014; 77:305–312. [PubMed: 24519948]
15. Costerton JW, Stewart PS, Greenberg EP. Science. 1999; 284:1318–1322. [PubMed: 10334980]
16. Hall-Stoodley L, Costerton JW, Stoodley P. Nat Rev Micro. 2004; 2:95–108.
17. Høiby N, Bjarnsholt T, Givskov M, Molin S, Ciofu O. International Journal of Antimicrobial Agents. 2010; 35:322–332. [PubMed: 20149602]
18. Kollef MH, Afessa B, Anzueto A, et al. JAMA. 2008; 300:805–813. [PubMed: 18714060]
19. Percival SL, Suleman L, Vuotto C, Donelli G. Journal of Medical Microbiology. 2015; 64:323–334. [PubMed: 25670813]
20. Kandi V, Kandi S. Epidemiology and Health. 2015; 37:e2015020. [PubMed: 25968114]
21. Pelgrift RY, Friedman AJ. Advanced Drug Delivery Reviews. 2013; 65:1803–1815. [PubMed: 23892192]
22. Miller KP, Wang L, Benicewicz BC, Decho AW. Chemical Society Reviews. 2015; 44:7787–7807. [PubMed: 26190826]
23. Schaeublin NM, Braydich-Stolle LK, Schrand AM, Miller JM, Hutchison J, Schlager JJ, Hussain SM. Nanoscale. 2011; 3:410–420. [PubMed: 21229159]
24. Fröhlich E. International Journal of Nanomedicine. 2012; 7:5577–5591. [PubMed: 23144561]
25. Kim ST, Saha K, Kim C, Rotello VM. Accounts of chemical research. 2013; 46:681–691. [PubMed: 23294365]
26. Li X, Kong H, Mout R, Saha K, Moyano DF, Robinson SM, Rana S, Zhang X, Riley MA, Rotello VM. ACS Nano. 2014; 8:12014–12019. [PubMed: 25454256]
27. Boda SK, Broda J, Schiefer F, Weber-Heynemann J, Hoss M, Simon U, Basu B, Jahnen-Dechent W. Small. 2015; 11:3183–3193. [PubMed: 25712910]
28. Vinoj G, Pati R, Sonawane A, Vaseeharan B. Antimicrobial Agents and Chemotherapy. 2015; 59:763–771. [PubMed: 25403677]
29. Li X, Yeh YC, Giri K, Mout R, Landis RF, Prakash YS, Rotello VM. Chemical Communications. 2015; 51:282–285. [PubMed: 25407407]
30. Chua PH, Neoh KG, Kang ET, Wang W. Biomaterials. 2008; 29:1412–1421. [PubMed: 18190959]
31. Goodman CM, McCusker CD, Yilmaz T, Rotello VM. Bioconjugate Chemistry. 2004; 15:897–900. [PubMed: 15264879]
32. Arvizo RR, Miranda OR, Thompson MA, Pabelick CM, Bhattacharya R, Robertson JD, Rotello VM, Prakash YS, Mukherjee P. Nano letters. 2010; 10:2543–2548. [PubMed: 20533851]
33. Hostetler MJ, Templeton AC, Murray RW. Langmuir. 1999; 15:3782–3789.
34. Brust M, Walker M, Bethell D, Schiffrin DJ, Whyman R. Journal of the Chemical Society, Chemical Communications. 1994:801–802.
35. Yan B, Zhu ZJ, Miranda O, Chompoosor A, Rotello V, Vachet R. Anal Bioanal Chem. 2010; 396:1025–1035. [PubMed: 19911174]
36. Hayden SC, Zhao G, Saha K, Phillips RL, Li X, Miranda OR, Rotello VM, El-Sayed MA, Schmidt-Krey I, Bunz UHF. Journal of the American Chemical Society. 2012; 134:6920–6923. [PubMed: 22489570]
37. Zhao Y, Tian Y, Cui Y, Liu W, Ma W, Jiang X. Journal of the American Chemical Society. 2010; 132:12349–12356. [PubMed: 20707350]
38. Li X, Robinson SM, Gupta A, Saha K, Jiang Z, Moyano DF, Sahar A, Riley MA, Rotello VM. ACS Nano. 2014; 8:10682–10686. [PubMed: 25232643]
39. Abbaszadegan A, Ghahramani Y, Gholami A, Hemmateenejad B, Dorostkar S, Nabavizadeh M, Sharghi H. Journal of Nanomaterials. 2015; 2015:8.

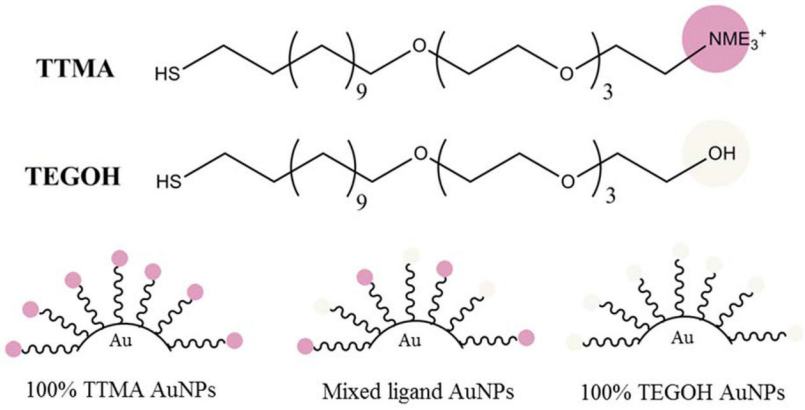

Figure 1.

Molecular structure of positive (TTMA) and neutral (TEGOH) ligands along with simplified structure of assembled gold nanoparticles (AuNPs) with differential composition of the two ligands.

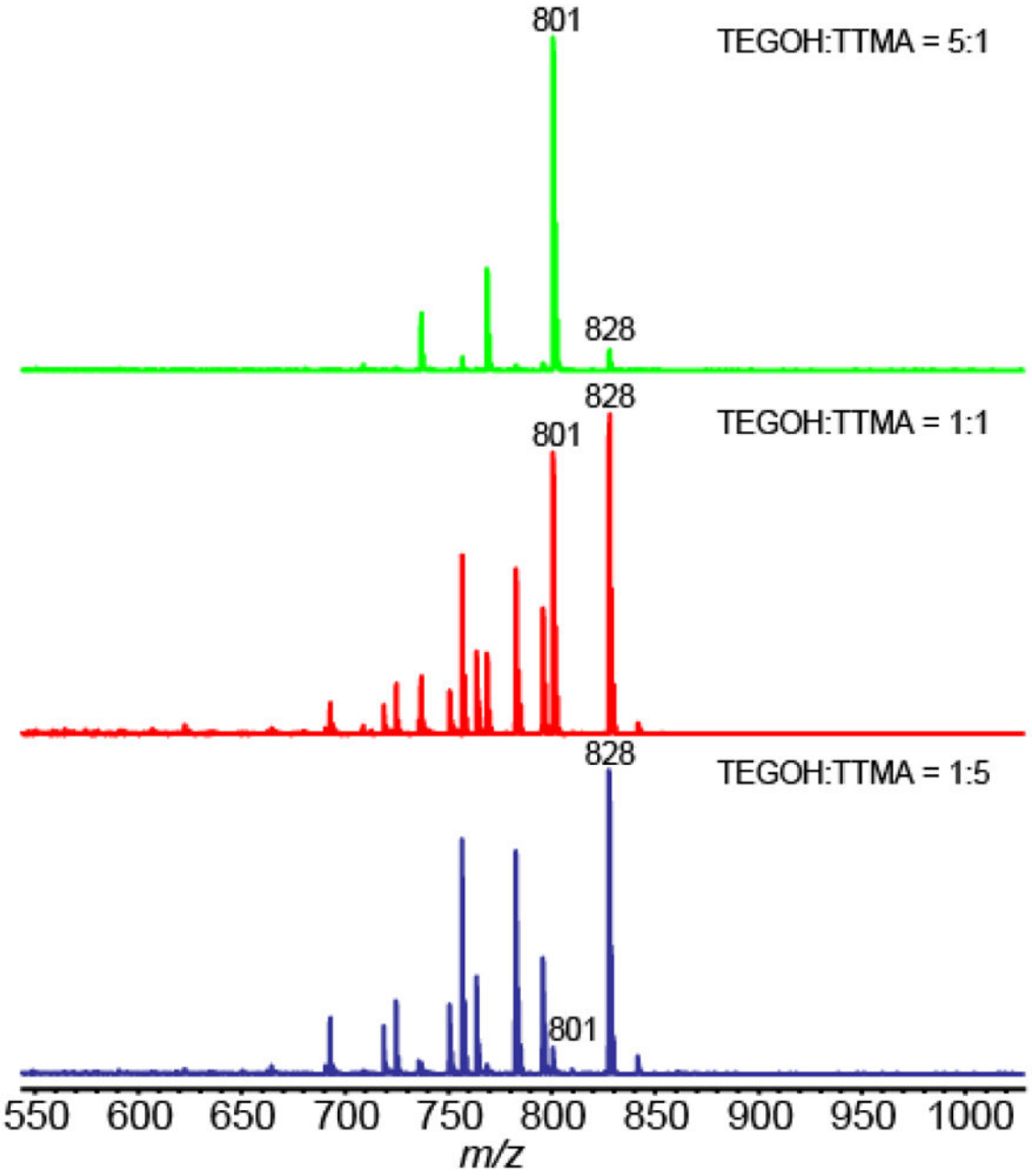

Figure 2.
LDI mass spectra of mixed monolayer protected AuNPs. The mass ratio of the TEGOH and TTMA ligands in the ligand-exchange reaction for each AuNP are also indicated.

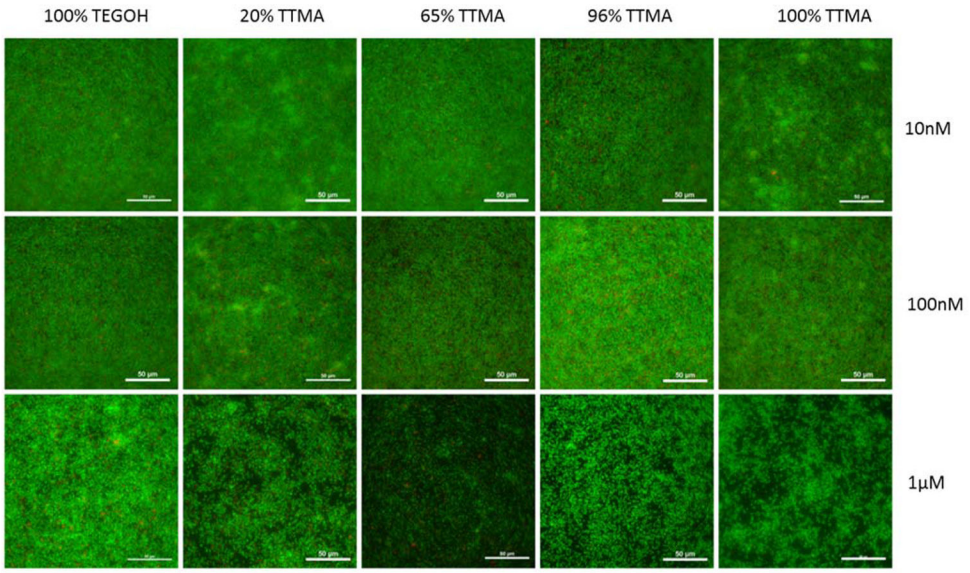

Figure 3.

Representative images of *S. aureus* biofilm stained with SYTO9 and propidium iodide (PI) after 24 h treatment with increasing concentrations of AuNPs. Panels are merged images of green (SYTO9, alive cells) and red (PI, dead/cell membrane compromised cells) channels. Scale bar= 50μm.

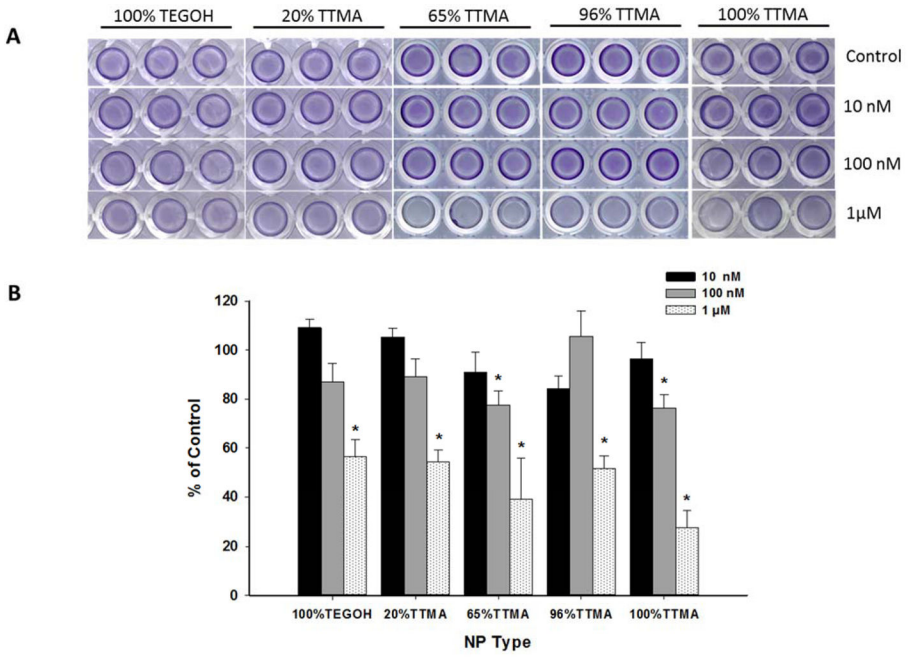

Figure 4.

Effect of varying concentrations of AuNPs on formation of *S. aureus* biofilm. A) Representative images of 48 h old bacterial biofilm stained with crystal violet. B) Quantification of biofilm after dissolving crystal violet in 70% ethanol. Values represent means ± SEM (N = 3 or 5), and * indicates significant difference between experimental and control groups (independent *t*-test, p-value <0.01).

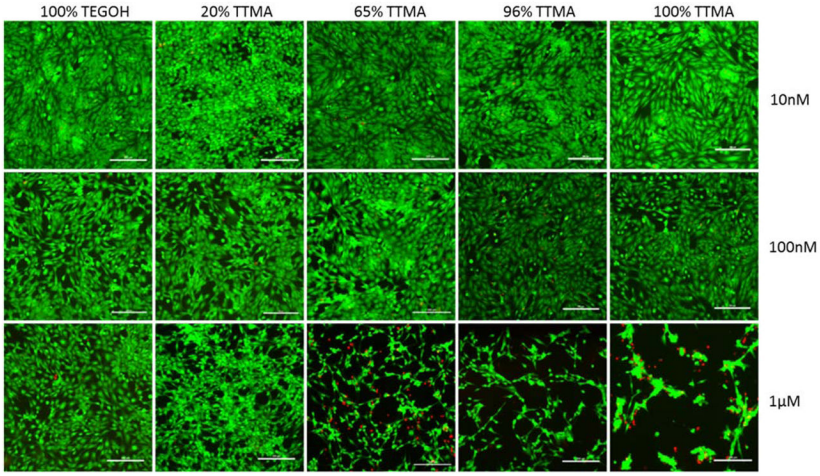

Figure 5.

Cytotoxic effect of AuNPs in human bronchial epithelial cells. Representative images of BEAS-2B cells treated with increasing concentration of AuNPs for 24 h and stained with calcein AM and EthD-1. Panels are merged images of the green (calcein, live cells) and red (EthD-1, dead/cell membrane compromised cells) channels. Scale bar= 200 μm.

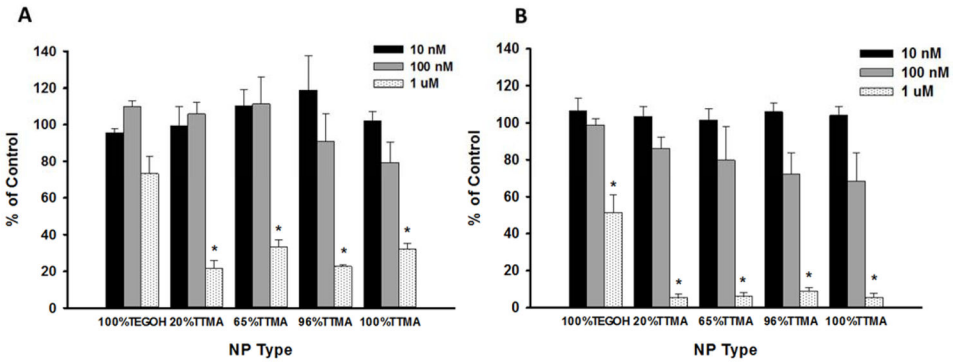

Figure 6.

Effect of AuNPs on proliferation of human bronchial epithelial cells. Cells were treated with increasing concentrations of AuNPs for A) 24 h or B) 48 h. Values represent mean ± SEM (N = 3 or 4) and * indicates significant difference between experimental and control groups (independent *t*-test, p-value <0.01).

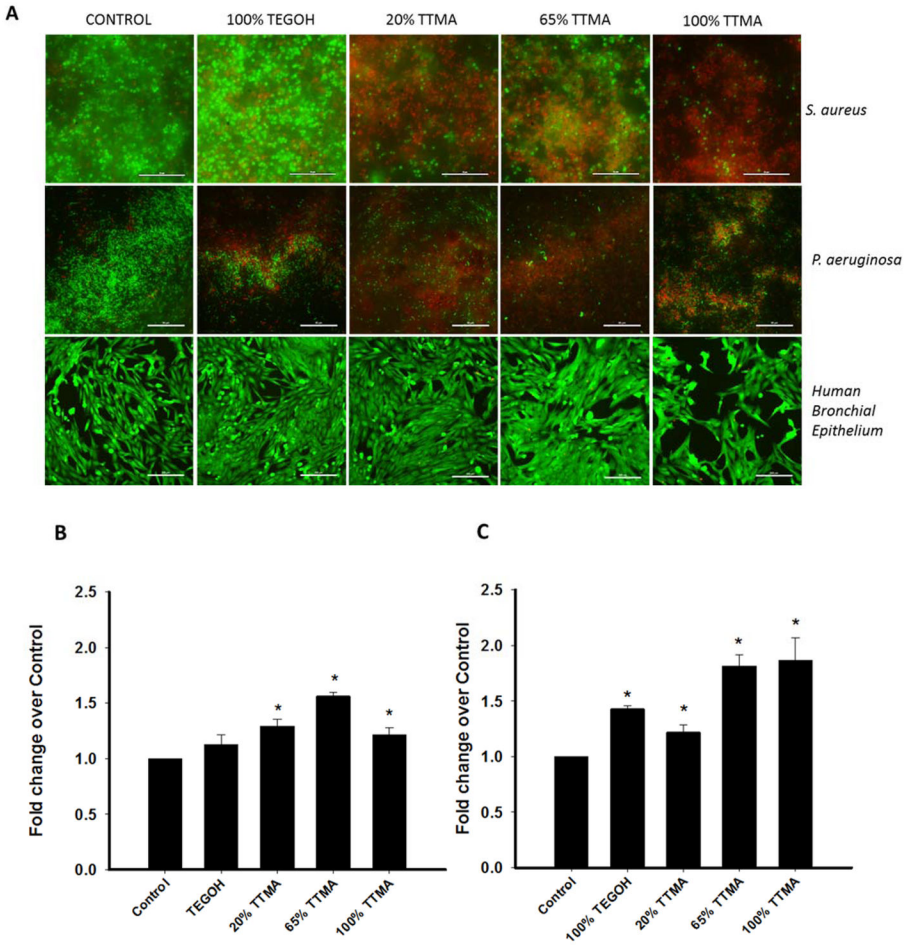

Figure 7.

AuNPs disrupts membrane integrity of *S. aureus* and *P. aeruginosa* cells but not of human epithelial cells. A) Cells were treated with 1 μM AuNP for 3 h along with SYTO9 and PI (for bacterial cells) or calcein AM and EthD-1 (mammalian cells). B) Quantification of LDHA release in the conditioned media after 6 h treatment with 1 μM AuNPs. C) LDHA release by *S. aureus* 6 h after AuNP treatment. Values represent mean + SEM (N=3 or 4) and * indicates significant difference between experimental and control groups (independent *t*-test, p-value <0.05).

Table 1

LDI-MS quantification of surface ligands on differentially charged AuNPs. Intensities of ions at m/z 801 and 828 shown in Figure 2 were used for the quantification.

Mass ratio of starting material (TEGOH/TTMA)	1:5	1:1	5:1
Mean of $I_{801}/(I_{801}+I_{828})$ by LDI-MS	0.061	0.46	0.94
SD	0.007	0.01	0.01
TEGOH percentage (%)	4%	35%	80%
TTMA percentage (%)	96%	65%	20%

Table 2

Zeta potential and DLS measurements of AuNPs in 5 mM sodium phosphate buffer adjusted to pH 7.4. Both measurements were performed using a Malvern Zetasizer Nano ZS after sonification.

Nanoparticle	Zeta potential (mV)	Diameter (nm)
100%TEGOH	1.2 ±5.3	11.5 ± 3.44 nm
20% TTMA	24.6 ± 5.1	10.4 ± 3.21 nm
65% TTMA	27.6 ± 9.4	11.6 ± 3.45 nm
96% TTMA	25.3 ± 5.2	10.2 ± 3.17 nm
100% TTMA	26.6 ± 7.5	11.5 ± 3.33 nm